Exploring the Contributions of Liquid-Phase Sulfur Chemistry to the Mass-Independent Sulfur Fractionation of the Archean Rock Record

by

Sebastian Hermann Kopf

B.S. Geosciences and Astrophysics

Jacobs University Bremen, 2008

Submitted to the Department of Earth, Atmospheric and Planetary Sciences

in partial fulfillment of the requirements for the degree of

Master of Science in Earth and Planetary Sciences

at the

MASSACHUSETTS INSTITUTE OF TECHNOLOGY

June 2010

Signature of Author: _____

Department of Earth, Atmospheric and Planetary Sciences
May 21, 2010

Certified by: _____

Shuhei Ono
Professor of Geochemistry
Thesis Supervisor

Accepted by: _____

Maria Zuber
E. A. Griswold Professor of Geophysics
Department of Earth Atmospheric and Planetary Sciences

Exploring the Contributions of Liquid-Phase Sulfur Chemistry to the Mass-Independent Sulfur Fractionation of the Archean Rock Record

by

Sebastian Hermann Kopf

Submitted to the Department of Earth, Atmospheric and Planetary Sciences
on May 21, 2010 in partial fulfillment of the
Requirements for the degree of Master of Science in
Earth and Planetary Sciences

ABSTRACT

Archean sulfur mass-independent fractionation (S-MIF) has been widely recognized as one of the strongest indicators for the rise of atmospheric oxygen in the Early Proterozoic. A decade after its discovery, the wide-ranging implications of Archean sulfur MIF have been discussed extensively and despite a number of recent studies on the gas-phase chemistry of sulfur, no definite overall picture has emerged to date as to the precise origin and preservation of the Archean mass-independent sulfur signal. The interpretation of the Archean sulfur MIF as a strong constraint for atmospheric oxygen levels, however, requires a dominant atmospheric source of sulfur MIF.

This study was aimed at investigating the potential contribution of the poorly explored mass-independent effects from liquid-phase sulfur chemistry and focused on sulfur isotope fractionation during liquid-phase photolytic breakdown of phenacylphenylsulfone (PPS) as a model system for initial investigation. Results confirm that MIF in this system is caused by the magnetic ^{33}S isotope and excludes other mechanisms such as nuclear volume effects or vibronic coupling that would produce concomitant MIF in the ^{32}S-^{34}S-^{36}S triad. This provides a starting point for discussing the implications of magnetic isotope effects as a mechanism for mass-independent isotope fractionation in the chemical evolution of the sulfur cycle and suggests that liquid-phase processes such as the photolysis of PPS cannot constitute the principal source of mass-independent sulfur fractionation in the Archean.

Thesis Supervisor: Shuhei Ono
Title: Professor of Geochemistry

1. Introduction

Variations in the relative abundances of the naturally occurring isotopes of sulfur have long been recognized as powerful tracers for biogeochemical processes throughout Earth's history [1] and have been used extensively for the study of numerous igneous, metamorphic, sedimentary, hydrothermal and biologic processes shaping the planet [2]. These thermodynamic, kinetic and biological processes all fractionate the four stable isotopes of sulfur (^{32}S, ^{33}S, ^{34}S and ^{36}S) in proportion to their differences in mass as predicted by the quantum mechanical theory of isotope fractionation [3-5], that is, they all produce a very specific mass-dependent isotope fractionation (MDF). Traditionally, studies have thus focused primarily on the more abundant ^{32}S and ^{34}S, with the rarer ^{33}S and ^{36}S both technically challenging to measure and generally believed to hold little additional information due to the mass scaling law. Strong deviations from this mass-dependent fractionation pattern were not expected to occur in the Earth's surface environment, as no relevant processes though capable of causing such an anomaly were known. However, just a decade ago, Farquhar et al. [6] first reported that many sedimentary sulfide and sulfate minerals from the Archean and Early Proterozoic older than ~2.4 billion years exhibit isotopic compositions that deviate strongly from the mass-dependent fractionation line. Traditional geochemical processes and sulfur cycling cannot readily explain these large deviations. Over half a century after Urey's 1947 [4] landmark paper on classical isotope effects, this observation thus opened up an entirely new area of study in sulfur isotope geochemistry related to mass-independent fractionation (MIF).

The origin of the MIF effects was hypothesized to be atmospheric [6] and modeling studies on the constraints for preserving such an atmospheric MIF signal in the rock record have since provided evidence for a mostly anoxic Archean atmosphere and rise of atmospheric oxygen above 10^{-5} times the present atmospheric level (PAL) only after ~2.3 Ga [7]. By today, the disappearance of sulfur MIF from the rock record is widely recognized as one of the most reliable proxies for the rise of atmospheric oxygen in the Early Proterozoic [2, 6-12], however, the processes and exact mechanisms of mass-independent sulfur fractionation in the Archean remain poorly understood.

With a large number of gas-phase mass-independent processes as well as unconventional mass-dependent effects for the oxygen ^{16}O –^{17}O – ^{18}O triad produced in laboratory studies as early as 1983 [13] and already fairly well studied [14, 15], similar effects were suspected to exist for the sulfur system. A number of gas phase processes for potentially relevant sulfur gases have since been investigated both theoretically and experimentally, such as SO_2 [9, 16-18], H_2S [19], OCS [20] and SO_3 [21] photolysis as well as CS_2 photopolymerization [22], S_3 recombination [23] and non-statistical reactions [17] and more recently, non gas-phase reactions and mechanisms such as surface adsorption [24], thermochemical sulfate reduction [25] and fluorination of metal sulfides [26]. However, while greatly advancing our understanding of these processes, no definite overall picture has emerged to date as to the precise origin and preservation of the Archean mass-independent sulfur signal, highlighting the importance to extend the search for potentially relevant sulfur MIF beyond the usual suspects.

To this date, particularly little attention has been granted to liquid phase processes, largely due to the lack of known mechanisms for mass-independent fractionation of ^{36}S. A study by Step et al. [27] investigated liquid-phase photolysis of phenacylphenylsulfone (PPS) for its sensitivity to magnetic field effects, but in the process also observed it to produce mass-independent ^{33}S fractionation in two measurements of the ^{32}S –^{33}S – ^{34}S triad (^{36}S could not yet be measured at the time). They hypothesized the effect to be spin-selective in nature, i.e. a magnetic isotope effect that fractionates the magnetic ^{33}S isotope mass-independently, but remarked the observed fractionation to be unexpectedly weak for a magnetic isotope effect. The system furthermore produced this isotope effect while operating at a light of 280-350nm without the need for UV-C radiation, allowing for this process to take place in the presence of weak ozone shielding in an already slightly oxic atmosphere, potentially removing the constraint on atmospheric oxygen imposed by gas-phase MIF. Without the need for short-wave UV light, this mechanism would even be unimpeded in the presence of strong organic shielding in an organic rich atmosphere [28], which would interfere with most gas phase processes that can produce mass-independent fractionation in the sulfur system. Inspired by the experimental results from this earlier investigation, this study intends to mend the gap by exploring the quadruple sulfur isotope fractionation during liquid-phase UV photolysis of phenacylphenylsulfone (PPS) as a model system for initial investigation of liquid phase processes.

2. Materials and Methods

Phenacyl phenyl sulfone (PPS, CAS# 3406-03-9) was purchased from the rare chemicals library of Sigma-Aldrich (#S596736, marketed by the name 2-phenylsulfonyl acetophenone). No purification grade was provided by the manufacturer. A high purity GC standard (≥99.5%) of acetophenone (CAS# 98-86-2) was purchased from Fluka (42163). All other chemicals that were used in the experiments are off-the-shelf high grade laboratory chemicals from Sigma-Aldrich (HPLC grade for solvents, ACS grade for concentrated acids). Extra dry high purity compressed oxygen was acquired from AirGas.

Photolysis

Phenacyl phenyl sulfone (PPS) was dissolved in a micellar solution of sodium dodecyl sulfate (SDS) by continuous stirring at low heat for ~10 hours to prepare a stock solution of 1mM PPS in 100mM SDS. Aliquots of 120mL (i.e. 120μmol of PPS) were photolyzed in a ~120mL quartz flask for 0, 2.5, 7.5, 12.5 and 17.5 minutes of light exposure from the full spectrum of a 150W Xenon lamp (Newport model 6254) as well as with the truncated spectrum from the same lamp using a glass filter to avoid radiation below λ=280nm (similar to the light regime used in the original experiment by Step et al. [27]). Concentration of PPS before and after photolysis was measured at λ=254nm on a Beckman Coulter System Gold HPLC (equipped with a Symmetry C18 5μm 4.6x250mm Column and 168 Diode Array Detector) using a methanol gradient.

Extraction

PPS and other hydrophobic reaction products were twice extracted from the micellar solution with a 4:1 mixture of ethyl acetate and dichloromethane, by carefully forming a 1:2 emulsion of the liquid solution with the solvent mix and separating the phases again by centrifugation. The solvent extract was evaporated to ~1mL, and PPS was isolated from other reaction products on a silica column using 3% isopropanol and 15% ethyl acetate in hexane as the eluent.

Combustion

The isolated PPS was crystallized from hexane and combusted with 900mg starch at 30atm O_2 in a Parr 1108 Oxygen Combustion Bomb [29] following the protocol developed by Arikawa and Sasaki [30]. 5mL of a 50g/L sodium carbonate solution was used as absorbent in oxygen bomb. The combustion with high pressure pure O_2 fully oxidizes the sulfur in PPS to sulfate, which dissolves in the sodium carbonate solution. The combustion capsule and all interior surfaces of the bomb were washed with copious amounts of deionized water. The washings were collected, acidified with 6M HCl to pH ~2 and spiked with 10mL bromine water to fully oxidize residual sulfur intermediates. After evaporation to ~50mL, the washings were filtered and barium sulfate was precipitated by addition of ~5mL 0.4M barium chloride. The barium sulfate precipitate was collected, washed with deionized water and dried for further processing. Combustion of starch blanks yielded no detectable barium sulfate.

Reduction

A mixture of hydroiodic, hypophosphorous and hydrochloric acid (Thode solution [1]) was used to reduce the collected barium sulfate to hydrogen sulfide [31]. The hydrogen sulfide was bubbled through a zinc acetate trap reacting quantitatively to form insoluble zinc sulfide, which was amended with ~5mL 0.1M silver nitrate to form silver sulfide after the reduction procedure. The silver sulfide was reacted over-night, washed several times with deionized water and dried for subsequent isotope analysis.

Analysis

Sulfur isotope ratio analysis of silver sulfide was carried out following the procedure described by Ono et al. [32]: 2mg samples of silver sulfide wrapped in aluminum were reacted with fluorine gas in externally heated nickel tubes at 300°C to form SF_6. After GC purification of SF_6, the $^{32}SF_5^+$, $^{33}SF_5^+$, $^{34}SF_5^+$ and $^{36}SF_5^+$ ions were analyzed by a Thermo-Electron MAT 253 isotope ratio mass-spectrometer.

Notation

Sulfur isotope compositions are expressed in the conventional δ *[‰]* notation as deviations in isotope ratios with respect to the traditional reference standard of the troilite inclusion from the Cañon Diablo meteroite (CDT):

$$\delta^x S = \left(\frac{{}^x S / {}^{32} S_{sample}}{{}^x S / {}^{32} S_{reference}} - 1 \right) \times 1000 \qquad (2.1)$$

with *x = 33, 34 or 36*. Sulfur MIF is commonly reported using the capital delta notation, measuring deviations in $\delta^{33}S$ and $\delta^{36}S$ from their respective expected mass-

dependent values ($\delta^{33}S \approx 0.515\ \delta^{34}S$ and $\delta^{36}S \approx 1.9\ \delta^{34}S$ *[3, 33].* Several slightly differing definitions are in use. For simplicity, all MIF data in this study is reported using the linear capital delta notation appropriate for relatively small isotopic fractionations [17, 34]:

$$\Delta^{33}S = \delta^{33}S - 0.515\ \delta^{34}S \quad (2.2)$$

$$\Delta^{36}S = \delta^{36}S - 1.9\ \delta^{34}S \quad (2.3)$$

Fractionation factors are a common measure of the magnitude of an isotope effect between two reservoirs *A* and *B* at equilibrium and can be described as the ratio of isotopic ratios between the reservoirs:

$$^{x}\alpha_{A/B} = \frac{(^{x}S/^{32}S)_A}{(^{x}S/^{32}S)_B} = \frac{\delta^{x}S_A + 1000}{\delta^{x}S_B + 1000} \quad (2.4)$$

with *x = 33, 34 or 36.*

Error estimation

Overall yield of the experimental procedure from initial photolysis to recovery of silver sulfide was consistent across all samples with an average 47.5±9.4% recovery. Most losses occurred at the combustion step, which was tested carefully for isotope fractionation effects with cystein blanks. Despite non-quantitative recovery through the elaborate procedure, little mass-dependent drift was observed (see table 2.1). The error from extraction, combustion and reduction procedures in combination with errors from the fluorination analysis itself is estimated at 0.6‰ for $\delta^{34}S$ from quadruplicate cystein combustion as well as triplicate PPS controls. Errors in $\delta^{33}S$

and $\delta^{36}S$ are mass-dependently correlated, giving high confidence in the precision of $\Delta^{33}S$, $\Delta^{36}S$ with errors of 0.01‰ and 0.03‰ respectively. The error in PPS quantification was estimated from the error in slope and y-intercept of the calibration curve linear least squares fit and calculated to be 0.032mM.

Blank	$\delta^{34}S$ [‰]	$\Delta^{33}S$ [‰]	$\Delta^{36}S$ [‰]
Cystein1	27.8	-0.02	0.33
Cystein2	27.8	-0.02	0.22
Cystein3	27.3	-0.02	0.26
Cystein4	29.2	-0.01	0.24
PPS1	0.1	0.02	-0.11
PPS2	0.0	0.01	-0.14
PPS3	-0.1	-0.01	-0.13

Table 2.1: Sulfur isotope ratio analysis of commercial Cystein and PPS blanks by Parr bomb oxidation-fluorination method.

3. Results and Discussion

For both light regimes (with and without 280nm filter), the photolysis of PPS followed a first order decay (eq 3.1) as observed by Step et al. [27]. The first order rate constant k can be estimated from the negative slope of the linear plot of the natural logarithm of the PPS concentration $ln([PPS])$ vs. time t (figure 3.1), and was calculated to be $k_{full}=0.049\pm0.003\ min^{-1}$ (half-life: $14.1\pm0.7\ min$) and $k_{280}=0.037\pm0.001\ min^{-1}$ (half-life: $18.8\pm0.6\ min$) for full spectrum and 280nm filter photolysis respectively.

$$\frac{d[PPS]}{dt} = -k\,[PPS] \tag{3.1}$$

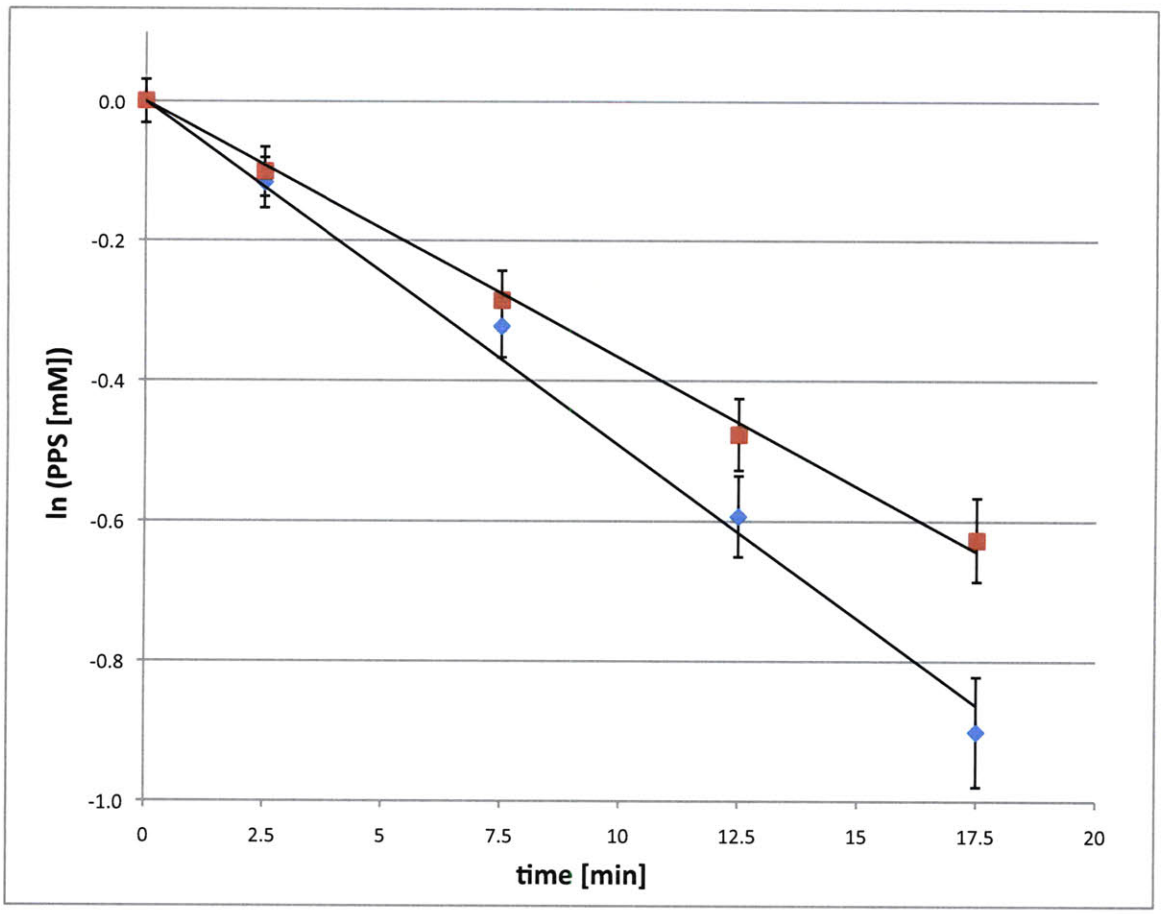

Figure 3.1: Plot of the natural logarithm of the PPS concentration vs. time during photolysis of PPS for full spectrum (blue) and >280nm filtered light regime (red). The slope of the plotted linear least squares fit signifies the negative first order rate constant of the reaction.

The good fit to a first-order reaction is in good agreement with the expected overall reaction mechanism for photolysis, as is the higher rate constant/faster decomposition for the full spectrum. However, given a peak in the absorption spectrum of PPS around *254nm* (data not shown), inclusion of λ*<280nm* light in the full spectrum is expected to increase the photolytic rate significantly more than the observed 1.3 fold. This result suggests that the photolytic rate of decomposition is

mostly limited by diffusion of the photolytic intermediates rather than photon absorption.

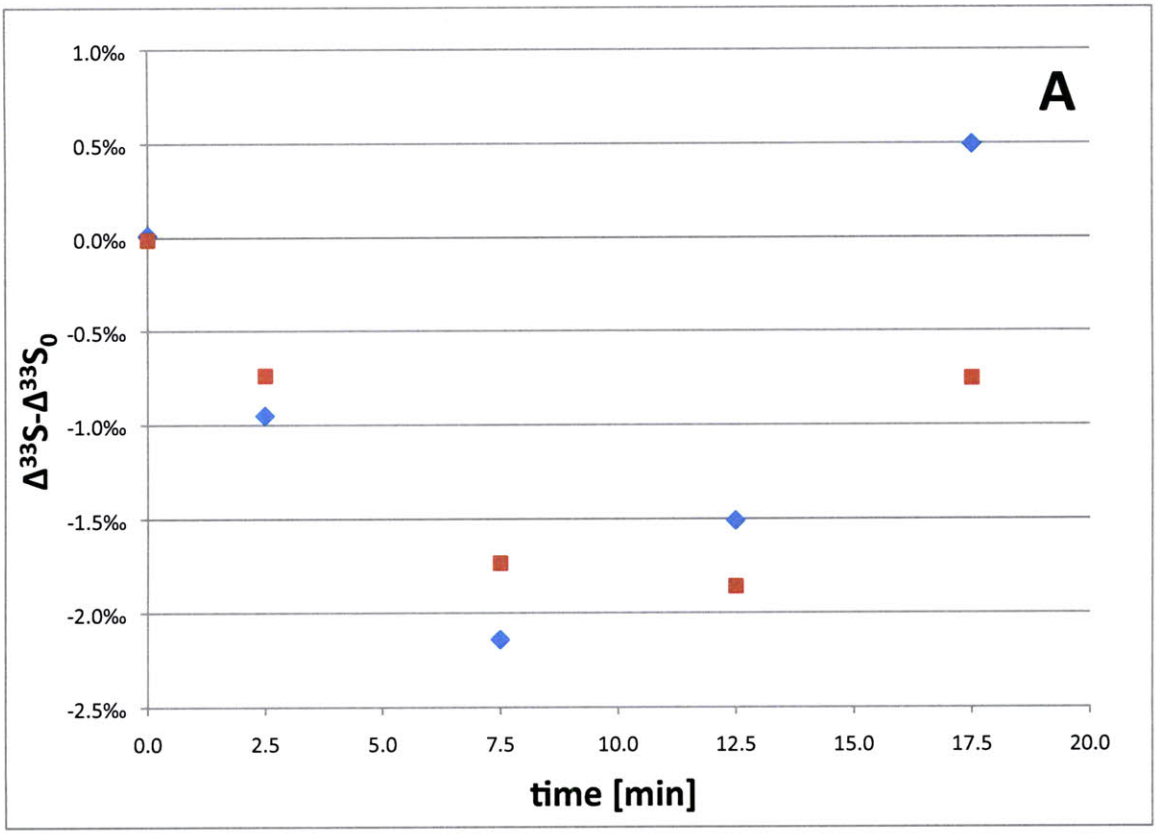

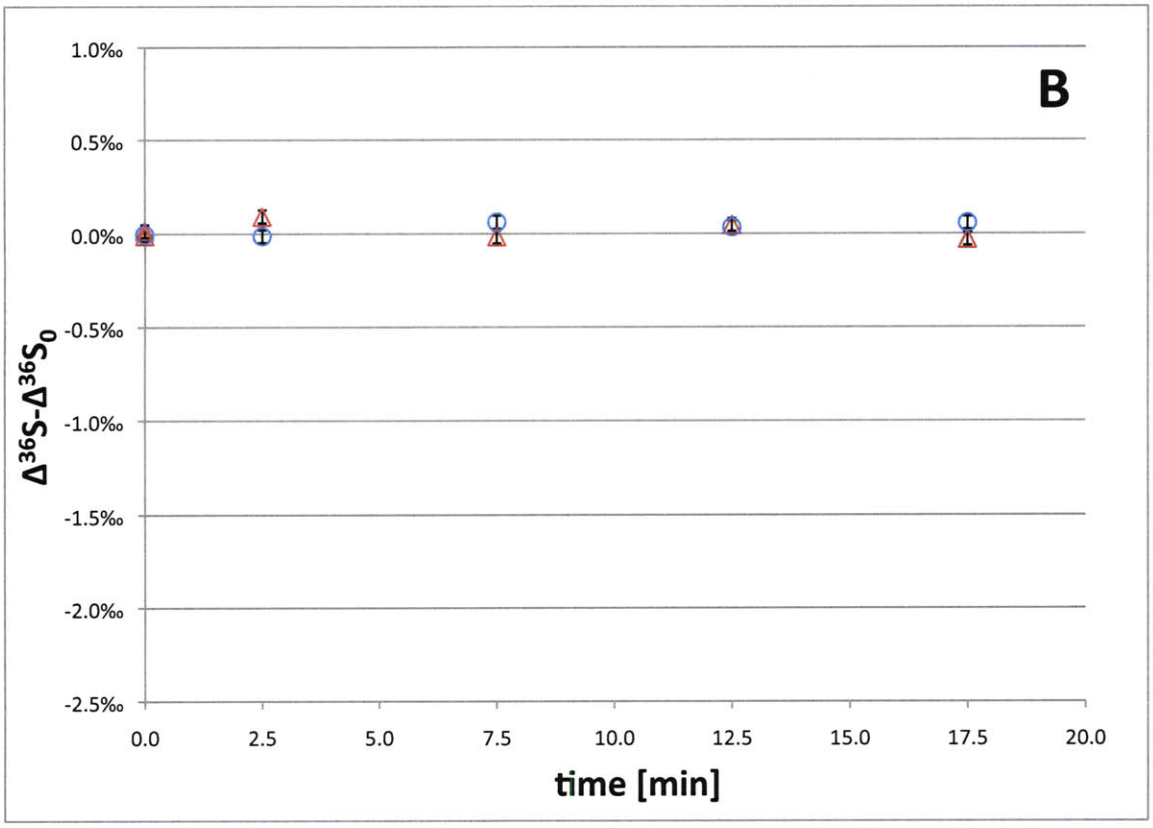

Figure 3.2: Plot of $\Delta^{33}S$ (A) and $\Delta^{36}S$ (B) in residual PPS (in comparison to initial $\Delta^{33}S_0$ and $\Delta^{36}S_0$) over the course of photolysis for full spectrum (blue) and >280nm filtered light regime (red). Uncertainties for these data are smaller than the symbol sizes.

Analysis of the sulfur isotope ratios in the residual PPS after photolysis provided high precision data to assess the mass-independent isotope fractionation (MIF) during photolysis of PPS. Figure 3.2 above shows the observed sulfur-MIF from PPS photolysis with full spectrum and >280nm filtered light regime. The results show that ^{33}S is indeed mass-independently fractionated while there is no ^{36}S MIF. This significant ^{33}S anomaly and consistent mass-dependent fractionation among the non-magnetic isotopes (^{32}S, ^{34}S, ^{36}S triad) rules out the presence of non-magnetic MIF effects and confirms the presence and importance of a magnetic isotope effect

(MIE) as suggested by Step et al. [27]. The implications of these results for the Archean sulfur isotope record will be addressed hereafter. A discussion of the surprising sign and shape of the $\Delta^{33}S$ signal and evaluation of the possible reaction mechanisms will follow.

Implications for Archean S-MIF

While it is intuitively understood quite readily that the MIF observed from PPS photolysis (high $\Delta^{33}S$ but $\Delta^{36}S \sim 0‰$) cannot account for Archean fractionation patterns, the following discussion proposes a quantitative method for rigorous comparative assessment of the potential role (or lack thereof) of such liquid photolytic processes or any other mechanism observed to create sulfur MIF.

The mass dependent fractionation line (*MDF*) in Cartesian sulfur space ($x=\delta^{33}S$, $y=\delta^{34}S$, $z=\delta^{36}S$) is defined more conveniently as vector $\overrightarrow{MDF} = (0.515 \quad 1 \quad 1.9)$, with a given sample of isotopic composition $\delta^{33}S$, $\delta^{34}S$, $\delta^{36}S$ plotting as the data point $\vec{S} = (\delta^{33}S \quad \delta^{34}S \quad \delta^{36}S)$. The cross product yields the direct relation to $\Delta^{33}S$ and $\Delta^{36}S$:

$$\overrightarrow{MDF} \times \vec{S} = \begin{pmatrix} 0.515 \\ 1 \\ 1.9 \end{pmatrix} \times \begin{pmatrix} \delta^{33}S \\ \delta^{34}S \\ \delta^{36}S \end{pmatrix} = \begin{pmatrix} \Delta^{33}S \\ 1.9\,\Delta^{33}S - 0.515\,\Delta^{36}S \\ -\Delta^{36}S \end{pmatrix} \qquad (3.1)$$

Assuming the isotopic composition of $\vec{S}$ to be a consequence of a number of classical isotope effects that have moved it along the mass dependent fractionation line $\overrightarrow{MDF}$ by a composite factor of k_0 as well as a number of N different mass-

independent effects[1] that have moved it along their specific fractionation lines $\overrightarrow{MIF_i}$ by a specific factor of k_i respectively, then $\vec{S}$ can be expressed as

$$\vec{S} = k_0 \overrightarrow{MDF} + \sum_i^N k_i \overrightarrow{MIF_i} \tag{3.2}$$

and equation 3.1 becomes (3.3)

$$\overrightarrow{MDF} \times \vec{S} = k_0 \overrightarrow{MDF} \times \overrightarrow{MDF} + \sum_i^N k_i \overrightarrow{MDF} \times \overrightarrow{MIF_i} = \begin{pmatrix} \sum_i^N k_i (MDF_y MIF_z - MDF_z MIF_y)_i \\ \sum_i^N k_i (MDF_z MIF_x - MDF_x MIF_z)_i \\ \sum_i^N k_i (MDF_x MIF_y - MDF_y MIF_x)_i \end{pmatrix}$$

Combing eq. 3.1 and 3.3 yields the following relation for the samples' $\Delta^{33}S/\Delta^{36}S$:

$$\frac{\Delta^{36}S}{\Delta^{33}S} = \frac{\sum_i^N k_i (MDF_y MIF_z - MDF_z MIF_y)_i}{\sum_i^N k_i (MDF_y MIF_x - MDF_x MIF_y)_i} \tag{3.4}$$

If multiple mass-independent effects with fractionation lines $\overrightarrow{MIF_i}$ and sample specific k_i influence the sample's isotopic composition, no clear correlation between $\Delta^{33}S$ and $\Delta^{36}S$ across a large sample size should emerge. However, if a single major mass-independent process $\overrightarrow{MIF_I}$ dominates the system ($k_I >> k_{I \neq i}$) by being the most ubiquitous effect, or possibly, the only signal that is preserved, eq. 3.4 can be simplified to yield a constant ratio m regardless of each sample's k_I:

$$\frac{\Delta^{36}S}{\Delta^{33}S} = \frac{MDF_y MIF_z - MDF_z MIF_y}{MDF_y MIF_x - MDF_x MIF_y} = m \tag{3.5}$$

$\Delta^{36}S$ and $\Delta^{33}S$ for a large number of Archean samples (plotted in figure 3.3) reveal a strong correlation with a correlation coefficient of *r=-0.94*. The correlation is not

[1] The term "mass-independent" in this context does not strictly refer to a mass-independent physical or chemical process but rather that to a process that is not mass-dependent in the sense of the MDF line. The process could still fractionate the isotopes with some non-traditional dependence on their mass.

perfect and possibly slightly skewed by a large number of samples with little MIF (clustered near the origin on the plot), but still strongly suggests the existence of a single process that largely dominated mass-independent sulfur fractionation during the Archean. It is evident that the liquid phase process observed from the experiments in this study (plotted concomitantly in figure 3.3) cannot constitute this single process. However, liquid phase UV photolysis together with other

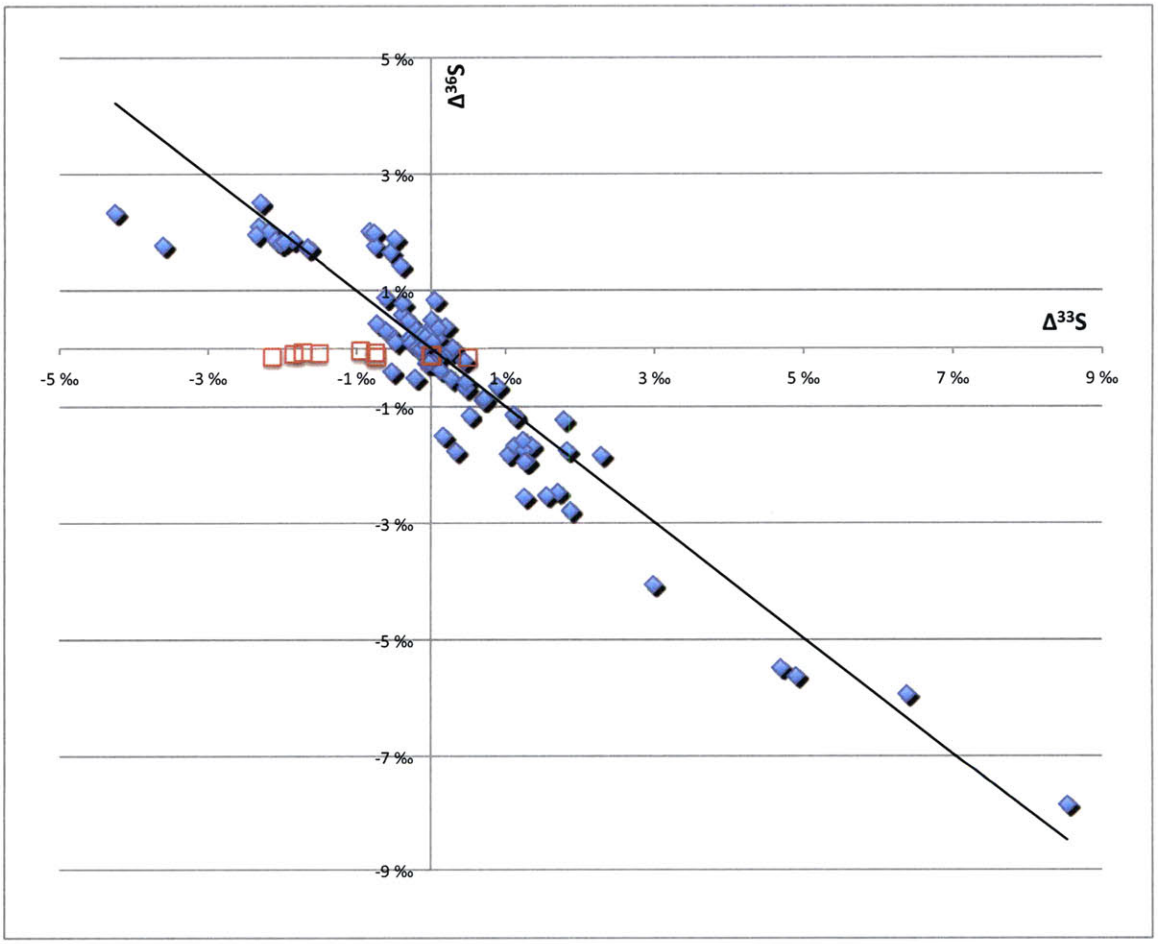

Figure 3.3: Plot of $\Delta^{36}S$ vs. $\Delta^{33}S$ for a number of Archean samples [12, 32] (blue diamonds, also includes some unpublished data) and samples from PPS photolysis (red squares, this study). The slope of the plotted linear least squares fit for the Archean

samples corresponds to the $\Delta^{33}S/\Delta^{36}S$ ratio m. Error bars are smaller than data point markers.

unconventional liquid and gas phase processes could provide smaller contributions to sulfur MIF, possibly causing the slight deviations from the main mass-independent fractionation line observed for Archean samples. Particularly, the liquid phase UV photolysis observed in this experiment does not produce significant mass-dependent fractionation ($\delta^{34}S \leq 1.2\pm0.6‰$, data not shown) and can thus overprint existing mass-dependent signals with MIF without altering the original MDF.

This above mentioned main mass-independent fractionation (MIF) line can be described by a vector for easy comparison much like the MDF line $\overrightarrow{MDF} = (0.515 \quad 1 \quad 1.9)$. Introducing the condition of $\overrightarrow{MIF}$ to be perpendicular to $\overrightarrow{MDF}$, eq. 3.5 and $\overrightarrow{MIF} \cdot \overrightarrow{MDF} = 0$ yield

$$MIF_x = MIF_y \frac{m\,MDF_x MDF_z - MDF_y{}^2 - MDF_z{}^2}{m\,MDF_y MDF_z + MDF_x MDF_y} \tag{3.6}$$

$$MIF_z = -MIF_y \frac{m\,MDF_x{}^2 MDF_z - MDF_x MDF_y{}^2 - MDF_x MDF_z{}^2}{m\,MDF_y MDF_z{}^2 + MDF_x MDF_y MDF_z} \tag{3.7}$$

Choosing $MIF_y=1$, the slope from the least squares linear fit of figure 3.3 ($m = -0.99\pm0.04$) provides an MIF vector of $\overrightarrow{MIF} = (4.06 \quad 1 \quad -1.63)$ indicating that whichever process dominates mass-independent fractionation enriches $\delta^{33}S$ over $\delta^{34}S$ while depleting $\delta^{36}S$. A planar projection of each sample data point $\vec{S} = (\delta^{33}S \quad \delta^{34}S \quad \delta^{36}S)$ onto a plane perpendicular to $\overrightarrow{MDF}$ and through $\overrightarrow{MIF}$ provides a useful visual representation (figure 3.4) of the scatter around this main

mass-independent fractionation line (represented by the x-axis) and illustrates how liquid phase photolysis as observed in this study could contribute to deviations from it.

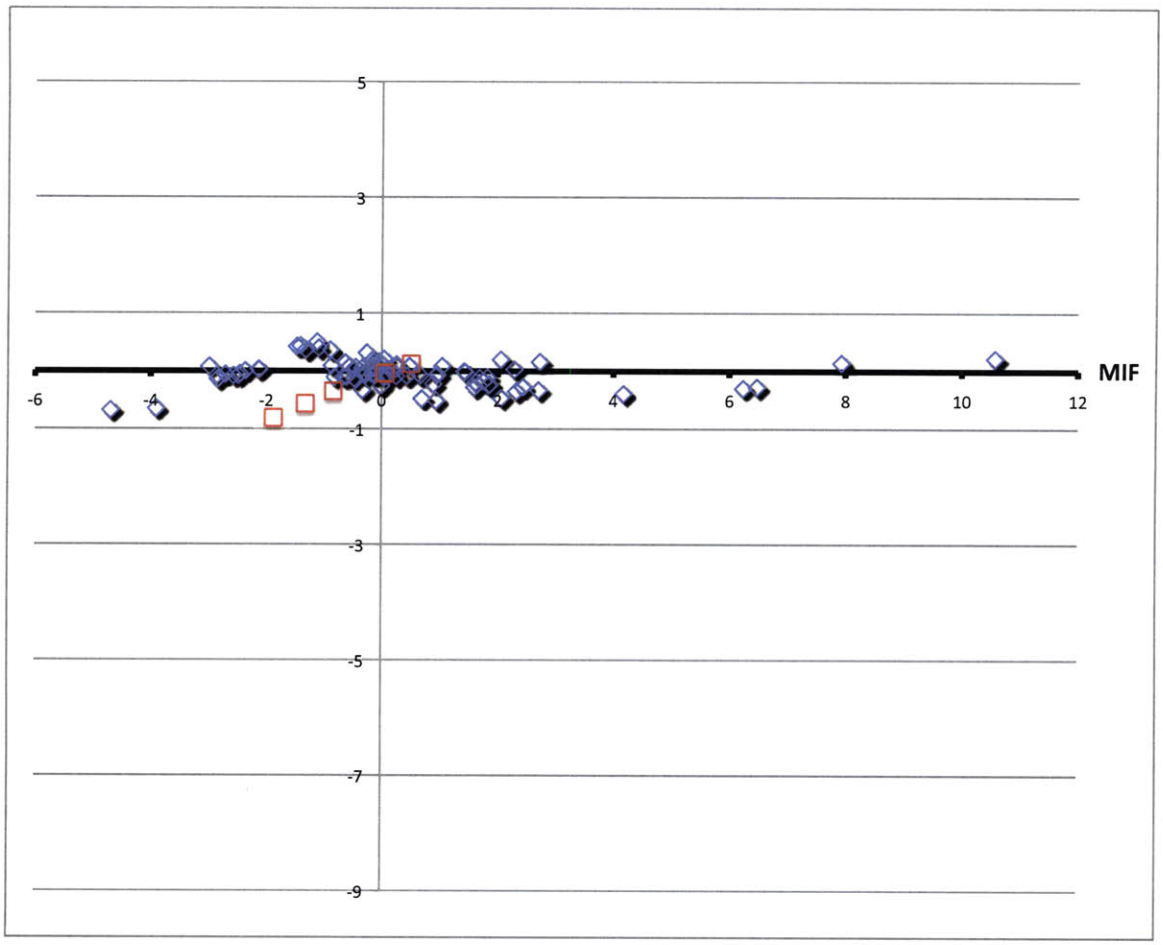

Figure 3.4: Planar projection of Archean samples (blue diamonds) and samples from PPS photolysis (red squares) onto a plane perpendicular to $\overrightarrow{MDF}$ *and through* $\overrightarrow{MIF}$*. X-axis represents the mass-independent fractionation line (normalized to a unit vector of* $\overrightarrow{MIF}$*) and y-axis represents perpendicular distance from* $\overrightarrow{MIF}$ *in the projected plane (normalized to perpendicular unit vector).*

Modeling PPS Photolysis

The clear lack of $\Delta^{36}S$ precludes liquid-phase processes such as PPS photolysis from posing as primary mass-independent effect for the generation of the Archean sulfur record and the exact shape and sign of the $\Delta^{33}S$ signal matters little for this interpretation. However, a more thorough understanding of the mechanism of PPS photolysis and the generation of the $\Delta^{33}S$ signal would provide valuable insight for a larger scale assessment of the potential scope and breadth of this intriguing effect and its contribution to deviations from the main MIF line.

The clear signal of a negative ^{33}S anomaly in the residual PPS, with $\Delta^{33}S$ values depleted as low as -2.14±0.01‰ was surprising as previous research [27] observed ^{33}S enrichment in the residual PPS. Not only the sign of the effect differs from previous results, the magnitude of the anomaly actually decreases and reverses with time, suggesting temporally changing contributions of at least two separate spin-selective processes. Rescaling the $\Delta^{33}S$ values for the different light conditions (full spectrum and >280nm) by the fraction of total PPS photolyzed at each time point ($1-e^{-kt}$) respectively reveals that they actually follow the same trajectory. This implies that the observed change in $\Delta^{33}S$ solely depends on the disappearance of PPS (or more likely, the concomitant appearance of reaction products), regardless of photolytic light regime (figure 3.5A). Mass balance considerations for the isotopic composition $\delta^{33}S\ (\Delta t)$ of the products *[dProd]* formed in the time interval Δt between the time points t_1 and t_2 , and the respective remaining *[PPS]* at t_1 and t_2 (eq 3.8) allow an estimate of the fractionation factor ${}^{33}\alpha_{PPS/dProd}\ (\Delta t)$ between the remaining

PPS and newly formed products during this time interval from experimental observations. (eq 3.8)

$$\delta^{33}S_{PPS}(t_2) \cdot [PPS](t_2) - \delta^{33}S_{PPS}(t_1) \cdot [PPS](t_1) = -\delta^{33}S_{dProd}(\Delta t) \cdot [dProd](\Delta t)$$

Plotted against the fraction of PPS photolyzed (i.e. product accumulated), the derived fractionation factors from the experimental results of this study as well as the measurements of Step et al. [27] reveal a strikingly linear correlation (figure 3.5B, correlation factor $R^2=0.97$, slope $m=1.017$, intercept $c=0.990$) indicating a linear dependence on the accumulation of reaction products which shifts the reaction pathway from ^{33}S depleting ($^{33}\alpha_{PPS/dProd} < 1$) to ^{33}S enriching ($^{33}\alpha_{PPS/dProd} > 1$) over the course of the experiment.

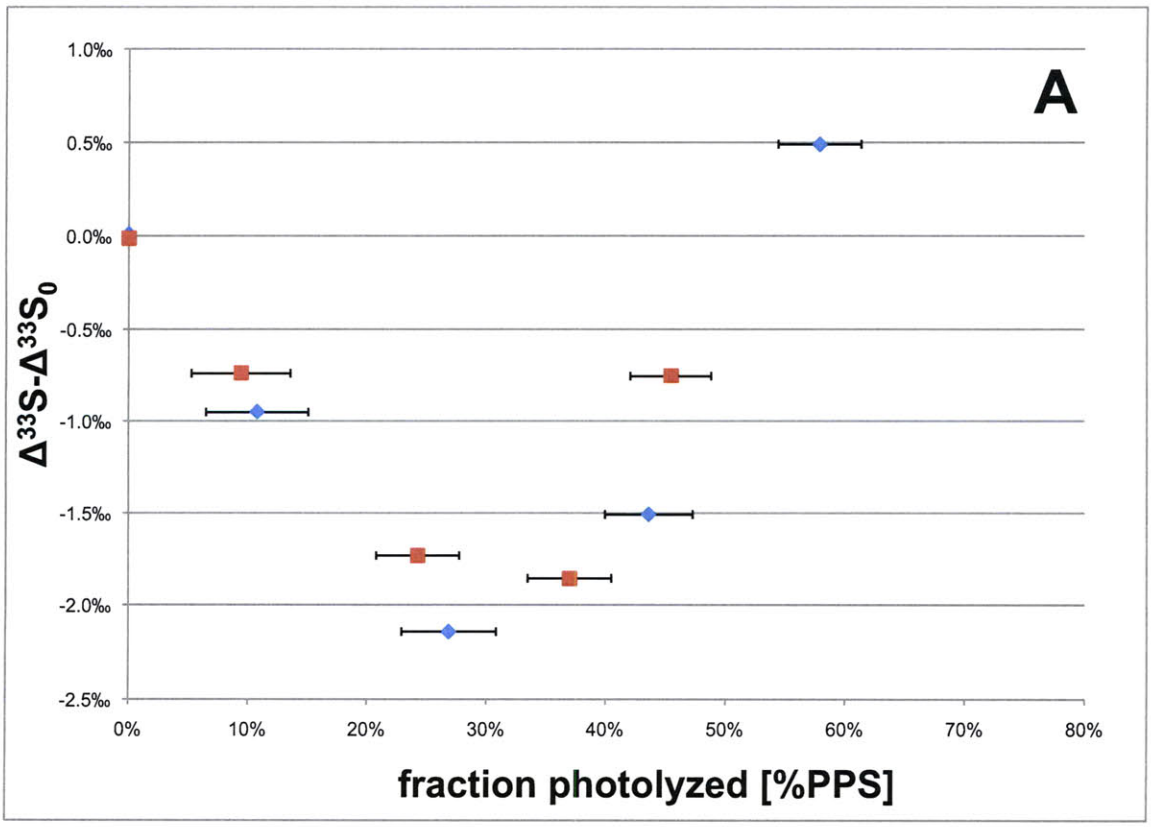

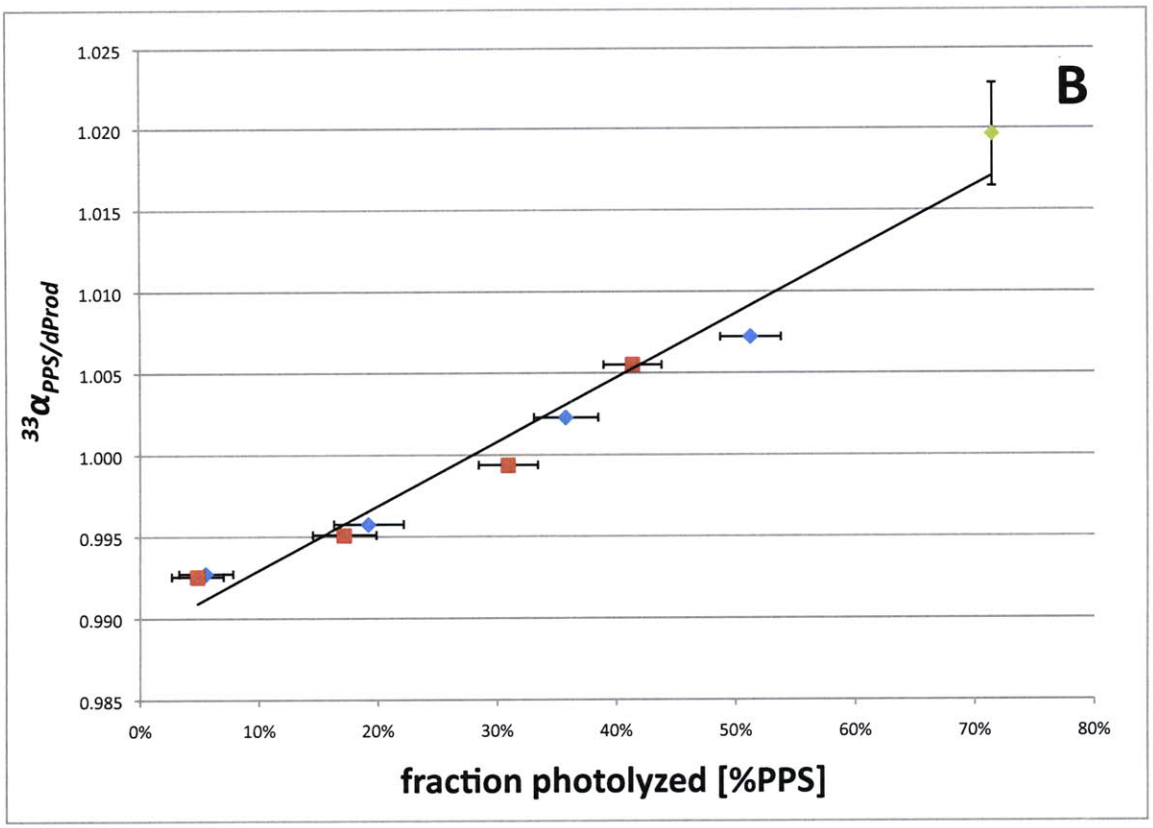

Figure 3.5: $\Delta^{33}S$ curve rescaled by the fraction of total PPS photolyzed (A). Fractionation factor $^{33}\alpha_{PPS/dProd}$ derived from experimental data (B). Data from full spectrum photolysis plotted in blue, >280nm filtered light regime in red. Green data point derived from Step et al. [27]. Vertical error bars for data from this study are smaller than symbol sizes. Horizontal error bar for data from Step et al. [27] is not known.

A number of reaction pathways both physically possible and capable of producing ^{33}S depletion through spin-selective processes, were considered in an attempt to elucidate the mechanism of PPS photolysis and identify the source of the observed linear dependence of $^{33}\alpha_{PPS/dProd}$ on product accumulation. Schematic illustrations of the three reaction pathways for PPS photolysis that are discussed in more details

hereafter are presented in figure 3.6. In the most simple model (3.6 A), PPS absorbs a photon to produce the electronically excited singlet state ^{1}PPS, which undergoes rapid intersystem crossing through spin-orbit coupling (SOC) to triplet ^{3}PPS (summarily represented by the excitation rate constant k_{ex}). At this point the ketone breaks at the weak carbon-sulfur bond to form a triplet state radical pair consisting of benzoylmethyl and phenylsulphonyl radicals. The radical pair at this point either separates completely and reacts to form a number of products such as acetophenone, sulfinic acids and other products (complete separation rate k_{sp}), or if paired for long enough, undergoes triplet-singlet intersystem crossing (ISC) through electron-nuclear hyperfine interactions (HFI) to singlet ground state and recombines to form PPS (recombination rate $^*k_{rc}$ [2]). The hyperfine interaction of the magnetic 33S nuclei will accelerate triplet-singlet conversion of radical pairs in which it is contained, increasing its abundance in the regenerated ketone [27]. These hyperfine interactions couple electron spin to nuclear spin and thus lead to increased recombination rates only for the magnetic ^{33}S isotope (the only naturally occurring sulfur isotope with nuclear spin). Reaction scheme A poses the most straightforward and intuitive model for PPS photolysis, however it can only lead to mass-independent enrichment of ^{33}S in residual PPS, not depletion.

---

[2] Rate constants marked with *, such as $^*k_{rc}$, indicate a process that can fractionate ^{33}S mass-independently.

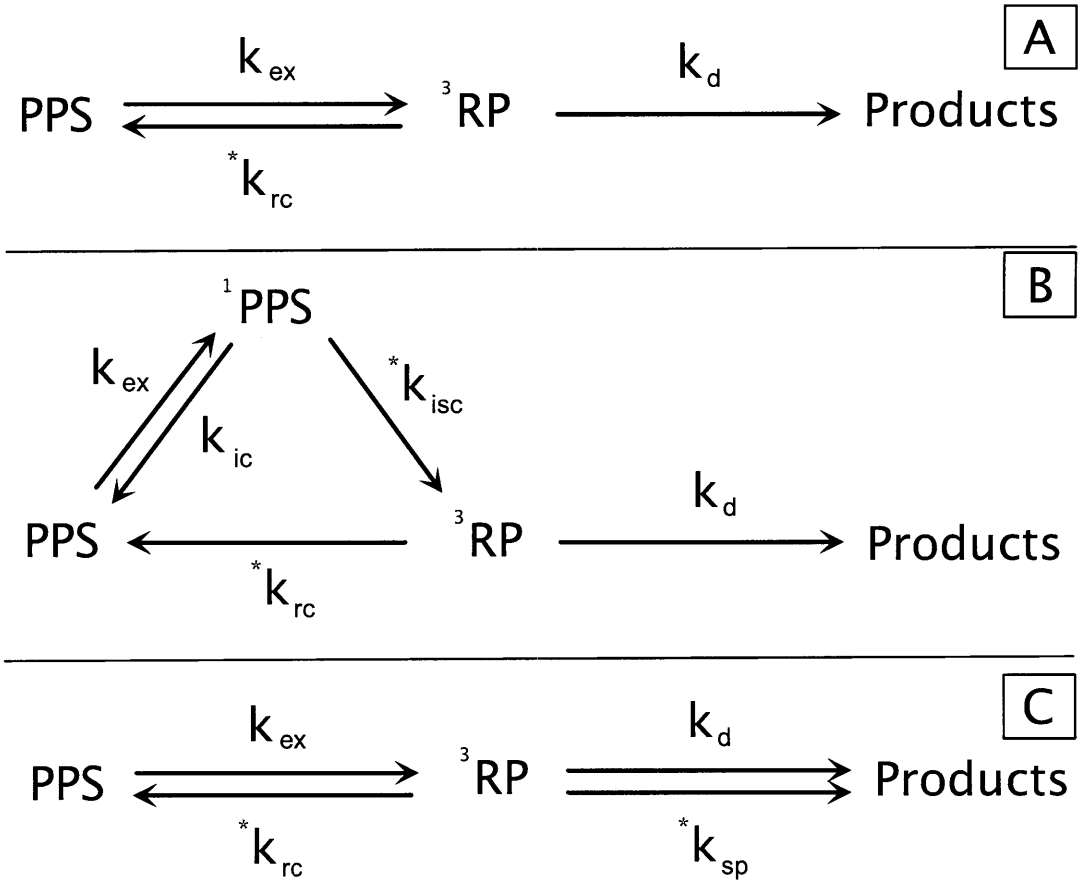

Figure 3.6: Discussed reaction schemes. A: most simple reaction scheme illustrating the overall process, cannot produce negative $\Delta^{33}S$. B: alternative reaction scheme that could produce the observed $\Delta^{33}S$ signal but is photochemically unlikely. C: modeled reaction scheme that is proposed as the most likely pathway.

Since intersystem crossing through spin orbit coupling (ISC through SOC) usually occurs at a rate on the order of 10^9 to 10^{12} s^{-1} [35] Step et al. [27] estimate spin-selective intersystem crossing through hyperfine interactions (ISC through HFI) in the experiment to occur at a rate of $7x10^7$ s^{-1}, it is conceivable that the ISC from excited singlet ^{1}PPS to triple ^{3}PPS (k_{ISC} in 4.5-B) could occur with a slight mass-

independent preference for the HFI accessible ^{33}S. The reaction pathway outlined schematically in figure 3.6-B illustrates this in detail (k_{ex} for electronic excitation to excited single ^{1}PPS followed by ISC $^{*}k_{ISC}$ to triplet ^{3}PPS). Without an escape pathway, this reaction scheme is identical to 4.5-A. However, if the excited singlet state ^{1}PPS can transition back to ground state through fluorescence or internal conversion (k_{IC}), the mass-independent ^{33}S depletion in ^{1}PPS can be preserved in the residual PPS. Relative changes in the rate constants of these different processes (for example as a consequence of product accumulation) could shift the net effect from depletion to enrichment (through the competing recombination pathway already introduced in 3.6-A) and indeed produce the observed $\Delta^{33}S$ curve. However, this can only succeeds if k_{IC} is significantly faster than $^{*}k_{ISC}$, which is kinetically difficult since Step et al. [27] observed no measurable fluorescence for PPS. Internal conversion and quenching could theoretically fill this role but are usually far slower than ISC. According to the energy gap law, internal conversion from first excited singlet ground state (k_{IC}) is usually significantly slower than 10^{8} s^{-1} for excitation energies greater than ~50 kcal/mol. Photons with a wavelength shorter than ~400nm (the upper limit likely involved in photoexcitation of PPS) carry energy in excess of 70 kcal/mol and both ketones and phenyl rings generally require even higher excitation energies beyond 80kcal/mol (~360nm), likely making internal conversion relatively too slow to compete with ISC. As previously mentioned, ISC through spin-orbit coupling (k_{SOC}) usually occurs at a rate of 10^{9} to 10^{12} s^{-1}: the structurally related benzophenone, for example, transitions from singlet to triplet state at 10^{11} s^{-1} [35]. This rate is possibly even faster for the sulfur-containing PPS as

spin-orbit interactions increase for heavier atoms scaling approximately with atomic number Z^4. This makes ISC most likely by far the most dominant escape pathway of excited singlet ^{1}PPS and reaction pathway 3.6-B unsuitable to produce the experimentally observed $\Delta^{33}S$ curve.

The third and final reaction pathway (illustrated schematically in figure 3.6-C and in more detail in figure 3.7) investigates an alternative pathway based on an alternative reaction mechanism proposed by Step et al. [27]. In this reaction scheme, photoexcitation and intersystem crossing to ^{3}PPS (k_{ex}) and spin-selective recombination ($^*k_{rc}$) proceed as proposed in 3.6-A. However, HFI-induced ISC of the triplet radical pair to ground state with subsequent recombination to PPS ($^*k_{rc}$) does not only compete with radical dissociation to form free radicals and subsequent products (k_{sp}), but also with radical separation and spin-selective (i.e. HFI-induced) ISC to form a singlet radical pair that recombines to form an unstable intermediate that cannot regenerate PPS and ultimately also forms reaction products ($^*k_{sp}$). As Step et al. [27] point out, the two different radical pairs differ mostly in the details of their diffusional history and possibly stereostructure in the micellar cage provided by the SDS solution. Consequently, it is indeed conceivable that their reaction rates are influenced differently by the accumulation of reaction products inside the micelle, thus shifting the equilibrium between the three escape pathways for ^{3}PPS ($^*k_{rc}$, k_{sp} and $^*k_{sp}$) over the course of photolysis. In order to elucidate the origin of the observed linear dependence of $^{33}\alpha_{PPS/dProd}$ on product accumulation, an analytical expression for $^{33}\alpha_{PPS/dProd}$ can be derived for this reaction pathway.

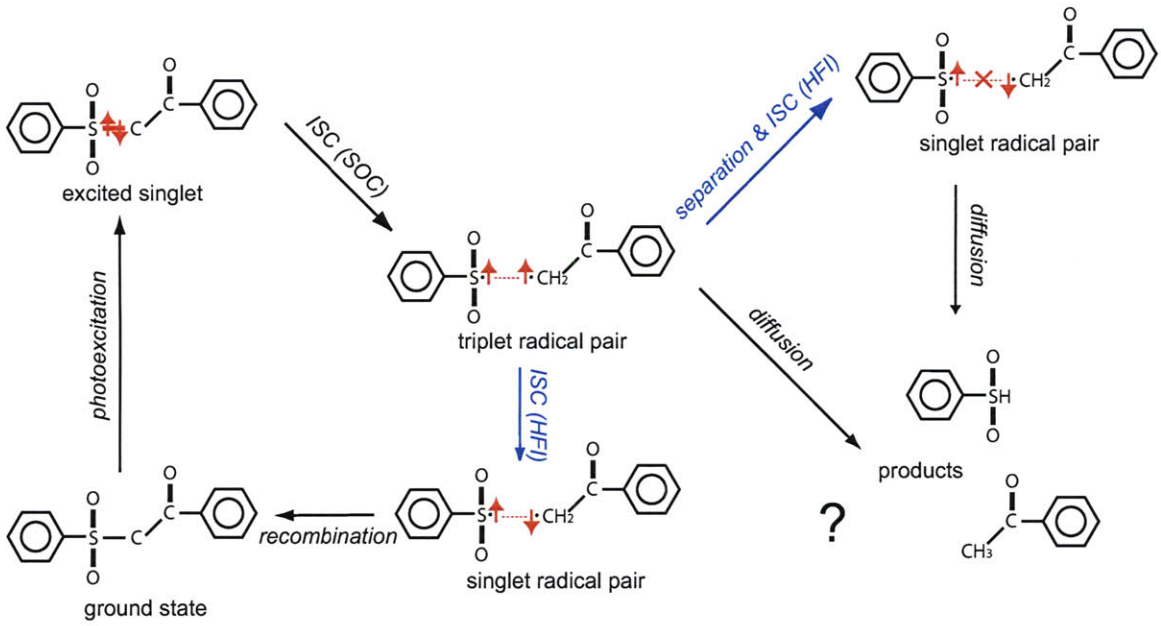

Figure 3.7: Simplified schematic of the most likely reaction pathway (illustrated in comparison with alternative pathways in figure 3.6). Red arrows indicate electron spin, blue arrows denote spin-selective reactions.

The fractionation factor $^{33}\alpha_{PPS/dProd}$ describes the relative fractionation for ^{33}S at any time t between the two reservoirs *PPS(t)* and d*Prod(t)*, an expression for this variable can be derived from the proposed reaction scheme (figure 3.6 C). The rate of change of concentration of the triplet state *[^{3}PPS]* and instantaneous products *d[Prod]* in this model is described by equations 3.9 and 3.10 below.

$$\frac{d[^3PPS]}{dt} = k_{ex}[PPS] - (^*k_{rc} + ^*k_{sp} + k_{sp})[^3PPS] \quad (3.9)$$

$$\frac{d[Prod]}{dt} = (^*k_{sp} + k_{sp})[^3PPS] \quad (3.10)$$

Assuming steady state and the concentration of the intermediate triplet state *[^{3}PPS]* thus to be constant, 3.9 can be substituted into 3.10 to directly relate *[PPS]* and *d[Prod]/dt*. Designating *[^{33}PPS]* and *[^{33}Prod]* as the concentration of ^{33}S containing

PPS and products respectively, $^{33*}k_{rc}$, $^{33}k_{sp}$ and $^{33*}k_{sp}$ as the respective rate constants of the ^{33}S containing species, $^{33}\alpha_{rc} = {}^{33*}k_{rc} / {}^{*}k_{rc}$ and $^{33}\alpha_{sp} = {}^{33*}k_{sp} / {}^{*}k_{sp}$ as the fractionation factors describing mass-independent fractionation during the spin-selective recombination and separation pathways, and recognizing that $^{33}k_{sp} \approx {}^{33}k_{sp}$ for the dissociative separation pathway in regards to mass-independent fractionation, we arrive at the following expression for the overall mass-independent ^{33}S fractionation factor $^{33}\alpha_{PPS\text{-}dProd}$ between PPS and instantaneous products: (3.11)

$$^{33}\alpha_{PPS-dProd}(t) = \frac{\frac{[^{33}PPS](t)}{[PPS](t)}}{\frac{d[^{33}Prod](t)}{d[Prod](t)}} = \frac{\frac{^{33*}k_{rc}+{}^{33*}k_{sp}+{}^{33}k_d}{{}^{*}k_{rc}+{}^{*}k_{sp}+k_d}}{\frac{^{33}k_{ex}\,(^{33*}k_{sp}+{}^{33}k_d)}{k_{ex}\,(^{*}k_{sp}+k_d)}} = \frac{(^{33}\alpha_{rc}\,\frac{^{*}k_{rc}}{^{*}k_{sp}} + {}^{33}\alpha_{sp} + \frac{k_d}{^{*}k_{sp}})(1+\frac{k_d}{^{*}k_{sp}})}{(\frac{^{*}k_{rc}}{^{*}k_{sp}} + 1 + \frac{k_d}{^{*}k_{sp}})(^{33}\alpha_{sp} + \frac{k_d}{^{*}k_{sp}})}$$

The presented form of eq. 3.11 illustrates well how the fractionation factor $^{33}\alpha_{PPS/dProd}$ is heavily influenced by the relative reaction rates of the three competing pathways. Knowing that $^{33}\alpha_{PPS/dProd}$ changes linearly with the accumulation products *[Prod]* ($^{33}\alpha_{PPS/dProd}$ = 0.990 + 1.017 *[Prod]*, see figure 3.5), and assuming that, for example, the relative rate of the recombination pathway $^{*}k_{rc}$ increases over the course of the experiment from an initial $^{*}k_{rc}^{0}$ with a linear dependence λ on the accumulation of reaction products *[Prod]* such that $^{*}k_{rc} = {}^{*}k_{rc}^{0} + \lambda[Prod]$, we can expand equation 3.11 and obtain the following two constraints on the reaction parameters:

$$0.990 = \frac{(^{33}\alpha_{rc}\,\frac{^{*}k_{rc}^{0}}{^{*}k_{sp}} + {}^{33}\alpha_{sp} + \frac{k_d}{^{*}k_{sp}})(1+\frac{k_d}{^{*}k_{sp}})}{(\frac{^{*}k_{rc}^{0}}{^{*}k_{sp}} + 1 + \frac{k_d}{^{*}k_{sp}})(^{33}\alpha_{sp} + \frac{k_d}{^{*}k_{sp}})} \quad (3.12)$$

$$1.017 = \frac{\lambda\left({}^{33}\alpha_{rc}\left(\frac{k_d}{{}^{*}k_{sp}}+1\right)-{}^{33}\alpha_{sp}-\frac{k_d}{{}^{*}k_{sp}}\right)\left(1+\frac{k_d}{{}^{*}k_{sp}}\right)}{\left(\frac{{}^{*}k^{0}_{rc}}{{}^{*}k_{sp}}+1+\frac{k_d}{{}^{*}k_{sp}}\right)^{2}\left({}^{33}\alpha_{sp}+\frac{k_d}{{}^{*}k_{sp}}\right)} \quad (3.13)$$

Due to the small number of constraints and the lack of experimental constraints on the large number of reaction parameters, the exact reaction dynamics can unfortunately not be modeled at this point. The origin of the observed linear dependence of ${}^{33}\alpha_{PPS/dProd}$ on product accumulation thus remains unresolved.

4. Conclusions

A decade after first evidence for the preservation of a strong mass-independent sulfur signal in the Archean rock record was published, its existence has been widely considered as one of the strongest indicators for the rise of atmospheric oxygen in the Early Proterozoic. The interpretation of the Archean sulfur MIF as a strong constraint for atmospheric oxygen levels requires a dominant atmospheric source of sulfur MIF. However, despite a number of recent studies on the gas-phase chemistry of sulfur, no definite overall picture has emerged to date as to the precise origin and preservation of the Archean mass-independent sulfur signal. This study was aimed at investigating the potential contribution of the poorly explored mass-independent effects from liquid-phase sulfur chemistry and focused on sulfur isotope fractionation during liquid, light regime dependent photolytic breakdown of phenacylphenylsulfone (PPS) as a model system for initial investigation. The results of this study provide evidence that liquid-phase processes such as the photolysis of PPS cannot constitute the principal source of mass-independent fractionation in the

Archean. However, such processes could provide a possible source for deviations from the main MIF line. These findings suggest liquid-phase sulfur processes to possibly play a minor, but most likely no major role in the creation of strong S-MIF and thus lend additional support to the hypothesis of a principal atmospheric source of sulfur MIF and the validity of its interpretation as a proxy for atmospheric oxygen. Future research in this field should focus on the investigation and identification of gas phase processes that can produce a mass-independent fractionation following the principal mass-independent fractionation line (as derived in this study) at environmentally relevant conditions.

5. Bibliography

1. THODE, H., J. MONSTER, and H. DUNFORD, *SULPHUR ISOTOPE GEOCHEMISTRY.* Geochim Cosmochim Ac, 1961. **25**(3): p. 159-174.

2. Mojzsis, S., et al., *Mass-independent isotope effects in Archean (2.5 to 3.8 Ga) sedimentary sulfides determined by ion microprobe analysis.* Geochim Cosmochim Ac, 2003. **67**(9): p. 1635-1658.

3. BIGELEISEN, J. and M. MAYER, *CALCULATION OF EQUILIBRIUM CONSTANTS FOR ISOTOPIC EXCHANGE REACTIONS.* J Chem Phys, 1947. **15**(5): p. 261-267.

4. UREY, H., *THE THERMODYNAMIC PROPERTIES OF ISOTOPIC SUBSTANCES.* J Chem Soc, 1947(MAY): p. 562-581.

5. Young, E., A. Galy, and H. Nagahara, *Kinetic and equilibrium mass-dependent isotope fractionation laws in nature and their geochemical and cosmochemical significance.* Geochim Cosmochim Ac, 2002. **66**(6): p. 1095-1104.

6. Farquhar, J., H. Bao, and M. Thiemens, *Atmospheric influence of Earth's earliest sulfur cycle.* Science, 2000. **289**(5480): p. 756-758.

7. Pavlov, A. and J. Kasting, *Mass-independent fractionation of sulfur isotopes in Archean sediments: Strong evidence for an anoxic Archean atmosphere.* Astrobiology, 2002. **2**(1): p. 27-41.

8. Farquhar, J., et al., *Isotopic evidence for Mesoarchaean anoxia and changing atmospheric sulphur chemistry.* Nature, 2007. **449**(7163): p. 706-U5.

9. Farquhar, J., et al., *Observation of wavelength-sensitive mass-independent sulfur isotope effects during SO2 photolysis: Implications for the early atmosphere.* Journal of Geophysical Research-Planets, 2001. **106**(E12): p. 32829-32839.

10. Farquhar, J. and B. Wing, *Multiple sulfur isotopes and the evolution of the atmosphere.* Earth and Planetary Science Letters, 2003. **213**(1-2): p. 1-13.

11. Kasting, J., *Earth history - The rise of atmospheric oxygen.* Science, 2001. **293**(5531): p. 819-820.

12. Ono, S., et al., *New insights into Archean sulfur cycle from mass-independent sulfur isotope records from the Hamersley Basin, Australia.* Earth and Planetary Science Letters, 2003. **213**(1-2): p. 15-30.

13. Thiemens, M. and J. HEIDENREICH, *THE MASS-INDEPENDENT FRACTIONATION OF OXYGEN - A NOVEL ISOTOPE EFFECT AND ITS POSSIBLE COSMOCHEMICAL IMPLICATIONS.* Science, 1983. **219**(4588): p. 1073-1075.

14. Gao, Y. and R. Marcus, *Strange and unconventional isotope effects in ozone formation.* Science, 2001. **293**(5528): p. 259-263.

15. Thiemens, M.H., *HISTORY AND APPLICATIONS OF MASS-INDEPENDENT ISOTOPE EFFECTS.* Annu Rev Earth Pl Sc, 2006. **34**(1): p. 217-262.

16. Lyons, A.R., *Photolysis of long-lived predissociative molecules as a source of mass-independent isotope fractionation: The example of SO2.* Adv Quantum Chem, 2008. **55**: p. 57-74.

17. Lyons, J.R., *Atmospherically-derived mass-independent sulfur isotope signatures, and incorporation into sediments.* Chemical Geology, 2009. **267**(3-4): p. 164-174.

18. Wing, B., J. Lyons, and J. Farquhar, *Experimental SO2 photochemistry and anomalous S isotope fractionation.* Abstracts of Papers of the American Chemical Society, 2004. **228**: p. U700-U700.

19. Farquhar, J., et al., *Evidence of atmospheric sulphur in the martian regolith from sulphur isotopes in meteorites.* Nature, 2000. **404**(6773): p. 50-52.

20. Lin, Y., M.S. Sim, and S. Ono, *Multiple-sulfur isotope effects during photolysis of carbonyl sulfide.* in preparation, 2010.

21. Pavlov, A., M. Mills, and O. Toon, *Mystery of the volcanic mass-independent sulfur isotope fractionation signature in the Antarctic ice core.* Geophys Res Lett, 2005. **32**(12): p. L12816.

22. Zmolek, P., et al., *Large mass independent sulfur isotope fractionations during the photopolymerization of (CS2)-C-12 and (CS2)-C-13.* J Phys Chem A, 1999. **103**(15): p. 2477-2480.

23. Francisco, J., J. Lyons, and I. Williams, *High-level ab initio studies of the structure, vibrational spectra, and energetics of S-3.* J Chem Phys, 2005. **123**(5): p. 054302.

24. Lasaga, A.C., et al., *Anomalous fractionation of sulfur isotopes during heterogeneous reactions.* Earth and Planetary Science Letters, 2008. **268**(1-2): p. 225-238.

25. Watanabe, Y., J. Farquhar, and H. Ohmoto, *Anomalous Fractionations of Sulfur Isotopes During Thermochemical Sulfate Reduction.* Science, 2009. **324**(5925): p. 370-373.

26. Cartigny, P., et al., *Experimental Evidence for Mass Independent Fractionation of Sulfur Isotopes Without any UV-photolysis or Glow Discharge.* Eos Trans. AGU 89 (53) Fall Meet. Suppl., Abstract V52B-03, 2008.

27. STEP, E., A. BUCHACHENKO, and N. TURRO, *MAGNETIC EFFECTS IN THE PHOTOLYSIS OF MICELLAR SOLUTIONS OF PHENACYLPHENYLSULFONE.* Chem Phys, 1992. **162**(1): p. 189-204.

28. Sagan, C. and C. Chyba, *The early faint sun paradox: Organic shielding of ultraviolet-labile greenhouse gases.* Science, 1997. **276**(5316): p. 1217-1221.

29. Company, P.I., *Operating Instructions No. 205M for the 1108 oxygen combustion bomb.* 2007: p. 1-12.

30. Arikawa, Y. and A. Sasaki, *Extraction and Isotope Measurement of Sulfur in Biological Samples.* 2006: p. 1-4.

31. FORREST, J. and L. NEWMAN, *AG-110 MICROGRAM SULFATE ANALYSIS FOR SHORT TIME RESOLUTION OF AMBIENT LEVELS OF SULFUR AEROSOL.* Analytical Chemistry, 1977. **49**(11): p. 1579-1584.

32. Ono, S., et al., *Mass-dependent fractionation of quadruple stable sulfur isotope system as a new tracer of sulfur biogeochemical cycles.* Geochim Cosmochim Ac, 2006. **70**(9): p. 2238-2252.

33. HULSTON, J. and H. THODE, *VARIATIONS IN S33 S34 AND S36 CONTENTS OF METEORITES AND THEIR RELATION TO CHEMICAL AND NUCLEAR EFFECTS.* J. Geophys. Res., 1965. **70**(14): p. 3475-&.

34. Ono, S., *Multiple-sulphur isotope biosignatures.* Space Sci Rev, 2008. **135**(1-4): p. 203-220.

35. J. Turro, N., V. Ramamurthy, and J. C. Scaiano, *Principles of molecular photochemistry: an introduction.* 2009: p. 495.